

Results: An emission spectrum resulting from electrical current injection through the *pn* junction is shown in Fig. 1(i), together with a PL spectrum (Fig. 1(ii)). An emission peaking at ~390nm is observed for both spectra. No other emission band is observed in the wavelength range 350–800nm. This UV emission band is thought to originate from excitons or electron hole plasma in ZnO because the peak position of the observed emission is fairly close to that of PL in ZnO, and no PL is observed for SCOs.

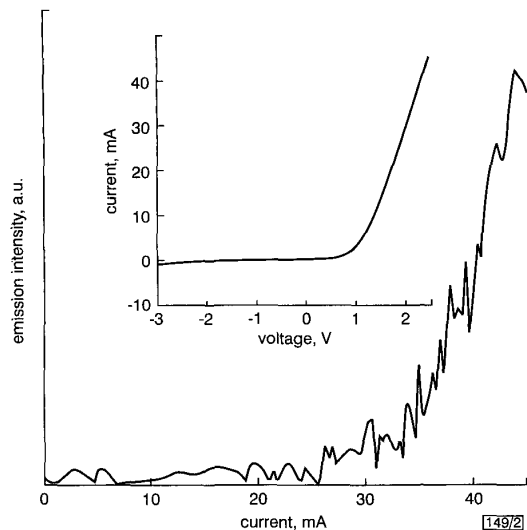


Fig. 2 Typical current-emission intensity characteristics of *p*-SrCu₂O₂/*n*-ZnO LED

Threshold current is ~30mA; turn-on voltage is ~1.0V
Inset: typical I-V characteristic

Fig. 2 shows the emission intensity against injection current. The tendency is similar to that of the current-voltage curve for the *pn* junction, as shown in the inset to the Figure, except that the threshold current (30mA) is significantly higher in the emission. The external efficiency of the emission is typically of the order of 0.01%. The low efficiency is most likely due to the degraded quality of the SrCu₂O₂ films deposited at low temperatures to avoid chemical reaction at the SCO/ZnO interface. Efforts to improve the device structure and fabrication processes are currently in progress, with the goal of increased efficiency. A concurrent study of EL spectra as a function of injected current is also in progress.

Acknowledgments: The authors would like to thank H. Kosuga of HOYA Corporation for assistance with reactive ion etching.

© IEE 2000
Electronics Letters Online No: 20000726
DOI: 10.1049/el:20000726

7 February 2000

H. Ohta, K. Kawamura, M. Orita, M. Hirano, N. Sarukura and H. Hosono (Hosono Project of Transparent ElectroActive Materials, ERATO, Japan Science and Technology Corporation, KSP C-1232, 3-2-1, Sakado, Takatsu-ku, Kawasaki-shi, 213-0012, Japan)

N. Sarukura: Also with Institute of Molecular Science, 38 Nishigonaka, Myodaiji, Okazaki 444-8585, Japan

H. Hosono: Also with Materials and Structures Laboratory, Tokyo Institute of Technology, Nagatsuta, Midori-ku, Yokohama 226-8503, Japan

References

- 1 KAWAZOE, H., YASUKAWA, M., HYODO, H., KURITA, M., YANAGI, H., and HOSONO, H.: 'P-type electrical conduction in transparent thin films of CuAlO₂', *Nature*, 1997, **389**, pp. 939–942
- 2 KUDO, A., YANAGI, H., HOSONO, H., and KAWAZOE, H.: 'SrCu₂O₂: A p-type conductive oxide with wide band gap', *Appl. Phys. Lett.*, 1998, **73**, pp. 220–222
- 3 THOMAS, D.G.: 'The exciton spectrum of zinc oxide', *J. Phys. Chem. Solids*, 1960, **15**, pp. 86–96
- 4 THOMAS, B.W., and WALSH, D.: 'Metal-insulator-semiconductor electroluminescent diodes in single-crystal zinc oxide', *Electron. Lett.*, 1973, **9**, pp. 362–363

- 5 KUDO, A., YANAGI, H., UEDA, K., HOSONO, H., KAWAZOE, H., and YANO, Y.: 'Fabrication of transparent p-n heterojunction thin film diodes based on entirely on oxide semiconductors', *Appl. Phys. Lett.*, 1999, **75**, pp. 2851–2853
- 6 OHTA, H., ORITA, M., TANJI, H., KAWAZOE, H., and HOSONO, H.: 'Heteroepitaxial growth of zinc oxide single crystal thin films on (111) plane YSZ by pulsed laser deposition', *Mat. Res. Soc. Symp. Proc.*, 1999, Vol. 570, pp. 309–313

Algorithm for high quality ionograms

F. Arikan, S. Salous and O. Arikan

A new ionogram algorithm, which is highly successful in generating robust and sharp digital ionograms free of artefacts and processing noise, is presented. An important feature of the algorithm is the distortionless zooming capability, which allows the user to concentrate only on the desired magnetoionic components of the ionogram.

Introduction: Digital ionograms are used in various applications ranging from automatic scaling to automatic link establishment [1]. These ionograms are generally cluttered with artificial artefacts and noise like components, which complicate automatic information extraction. The standard fast Fourier transform (with rectangular windows) introduces undesired spectral leakage in the form of high sidelobes [2]. Although the use of alternative windows such as the Blackman window partially eliminates the speckles due to spillovers, they also widen the mainlobe of the rectangular windowed periodograms [2–4]. In this Letter, a new ionogram algorithm, which makes use of efficient signal processing tools and eliminates the artificial artefacts due to hardware and the processing of data, is presented. The distortionless zooming capability facilitates the tracking of layers or modes. The performance of the ionogram algorithm is demonstrated using an experimental data set which is collected by the wideband frequency modulated continuous wave (FMCW) bistatic HF chirp sounder developed at the University of Birmingham [3]. The data set is obtained over a 273km great circle path in the UK by a frequency sweep of 4MHz generated in 4s with a sweep separation of 10s. The data were sampled with a 12-bit digital to analogue converter at a sampling rate of 16384Hz giving a total of 65536 samples per sweep. The fading envelope of the received signal is distorted by a high level of interference, which is usually present in the HF band. Since ionograms are obtained by dividing the received signal into sections prior to the spectral analysis, the effect of interference is to raise the noise floor in the section. The effect of interference can be reduced by clipping its level to a value equal to or higher than the peak of the signal [2]. This technique is generally tedious and a more automatic noise elimination technique is desirable. Such a technique is discussed in the following Section.

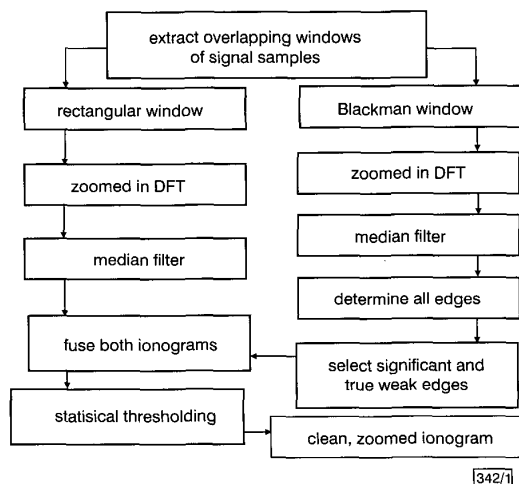


Fig. 1 Flowchart of new digital ionogram algorithm

Framework of ionogram algorithm: The algorithm for clean and sharp ionogram generation is presented in Fig. 1. The first step is to express the received chirp signal in the time-frequency plane. For this purpose, smaller data sequences will be extracted from the signal vector with an allowance of overlapping samples. The standard procedure in obtaining ionograms is to apply a rectangular window to the extracted data samples, pass them through a fast Fourier transform (FFT) algorithm and subsequently arrange the sequences in the time-frequency plane [3, 4]. The rectangular window is used despite its high sidelobe levels (the first sidelobe level is only 13.5dB down from the mainlobe) since it has the narrowest first null beamwidth compared with the other window functions [4]. To reduce the effects of sidelobes on the detection of echoes, other windows such as the Blackman window are used (its first sidelobe level is -57dB down from the mainlobe level). However, the mainlobe beamwidth of the Blackman window is three times that of the rectangular window. Thus it is desirable to combine the best of these two window functions, i.e. a sharp mainlobe and low spillovers. Therefore the extracted data samples are passed through both rectangular and Blackman windows separately. To transform the windowed signal sequences into the frequency domain, a discrete Fourier transform (DFT) is used. The advantages of using the DFT as opposed to a conventional FFT are two-fold. First, the DFT can be represented as a non-recursive chirp filter and thus this will lead to real-time computations of the DFT on a single chip. The second advantage of implementing the DFT as a chirp filter (i.e. a chirp z-transform) is the ability to concentrate or zoom into a desired section of the ionogram without any distortion. Fig. 2 shows the zoomed-in Blackman windowed and median filtered ionogram to observe the $1F_2$ -layer ordinary and extraordinary waves.

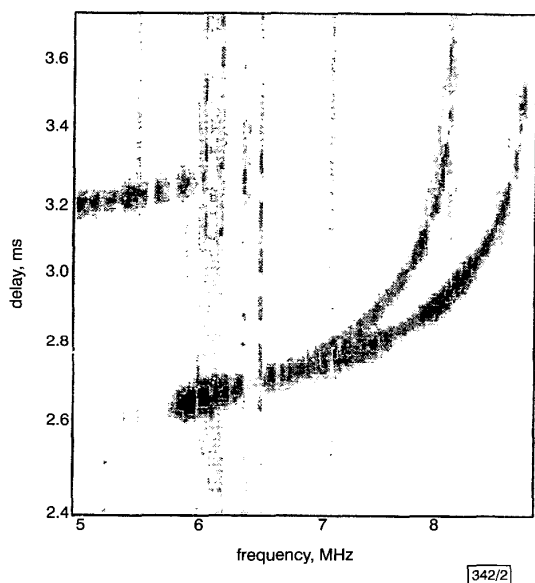


Fig. 2 Blackman windowed, median filtered and zoomed ionogram to observe $1F_2$ -layer ordinary and extraordinary waves

The third step of the ionogram generation is to discriminate between significant and insignificant signal transitions and to eliminate the insignificant signal components. The significant edges of the Blackman windowed and median filtered periodogram are determined using Canny's edge detection method. This method is quite robust to noise components and is highly successful in detecting true weak edges. After determining the locations of significant signal transitions, the median filtered Blackman windowed and rectangular windowed spectrum estimates are fused to obtain a sharp periodogram with negligible ringing. As a final step, a statistical thresholding method is used to partially eliminate the leftover artefacts and noise-like components. Fig. 3 presents a sharp and clean fused ionogram.

The success of this new ionogram algorithm is mostly determined by the proper choice of parameters such as the window length, the number of overlapping samples, the length of the DFT,

the median filter length, and the threshold levels used in determining the significant and insignificant signal transitions and statistical thresholding routine. To increase the resolution in the investigated spectral interval, the window length should be chosen to be as wide as possible, yet the analysed signal segment has to have negligible spectral variations inside the window. Choosing this window to be longer than its optimum length not only causes blurring in the estimated ionogram but also makes it difficult to resolve rapid variations around the critical frequency. Thus the choice of the optimum length is based on the restrictions of the ionospheric physics and it is set to 512 in the off-line analysis of the ionograms presented in this Letter. The optimum choice of the number of overlapping samples (which is set to 50% overlap in this analysis) is related to the window length and its value can be modified according to the characteristics of the operating link. If this parameter increases more than its optimum value, the resolution in the frequency axis decreases. The thresholds in the edge detection and statistical thresholding routines are also set according to the off-line analysis of ionograms. The decisions of significant or insignificant signal transitions are based on an expert point of view. Even if some insignificant traces are left after the edge detection routine is run, the statistical thresholding algorithm eliminates the leftover insignificant artefacts. All these parameters can be set once optimised over a specific link, and they can be adopted in the automatic selection of the parameters in an on-line analysis. Generally, once the parameters are set in an optimum or quasi-optimum manner, the ionogram algorithm is very robust to variations in the ionospheric conditions and high quality ionograms can still be generated.

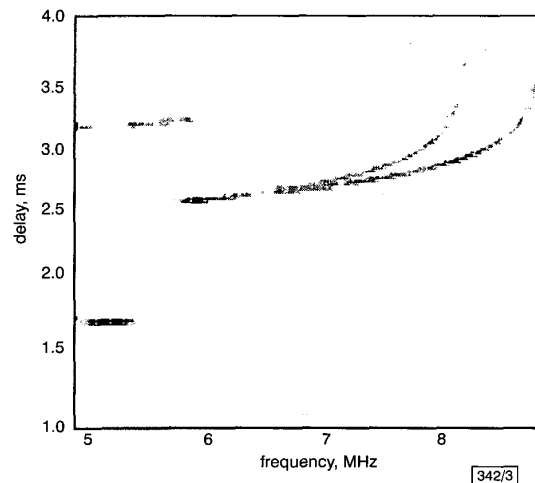


Fig. 3 Fused ionogram, sharp and free of noise and artefacts

Conclusion: An alternative digital ionogram algorithm, which is based on recent digital signal processing techniques, is presented. The performance of this new ionogram algorithm has been verified with HF chirp sounder data collected from an oblique midlatitude path. The presented algorithm is highly successful in obtaining robust and sharp ionograms free of artefacts and processing noise. This algorithm can also be modified to be used in real time (on-line) applications.

© IEE 2000

Electronics Letters Online No: 20000725
DOI: 10.1049/el:20000725

F. Arikan (Department of Electrical and Electronics Engineering, Hacettepe University, Beytepe, 06532, Ankara, Turkey)

E-mail: arikan@hacettepe.edu.tr

S. Salous (Department of Electrical Engineering and Electronics, UMIST, PO Box 88, Manchester M60 1QD, United Kingdom)

O. Arikan (Department of Electrical and Electronics Engineering, Bilkent University, Bilkent, 06533 Ankara, Turkey)

References

- GOODMAN, J.M.: 'HF communications-science and technology' (Van Nostrand Reinhold, New York, NY, 1992)

- 2 SALOUS, S.: 'On the potential applicability of auto-regressive spectral estimation to HF chirp sounders', *J. Atmospheric Solar-Terrestrial Phys.*, 1997, **59**, (15), pp. 1961-1972
- 3 SALOUS, S.: 'FMCW channel sounder with digital processing for measuring the coherence of wideband HF radio links', *IEE Proc. F*, 1986, **133**, (5), pp. 456-462
- 4 FANTE, R.L.: 'Signal analysis and estimation' (John Wiley and Sons, New York, NY, 1988)

Efficient wideband digital correlation

B.R. Carlson and P.E. Dewdney

A method is described for digital correlation of very wideband signals from a radio interferometer. The intent of the method is to achieve maximum spectral resolution at minimum cost. Data are digitally filtered and decimated into lower rate sub-bands which are separately cross-correlated and integrated before being seamlessly stitched together to yield the wideband spectrum. Simulation results are presented to enable a comparison to be made of this method with results obtained using a full band correlator.

Introduction: The use of high-speed samplers with clock rates that exceed those of downstream cross-correlation hardware requires a sub-rate demultiplexing scheme. Time-division demultiplexing methods have been developed, but in such methods many cross-correlations must be performed per spectral channel. In a large interferometer array, this adds significant cost to the system or reduces the number of spectral channels that could be available. On the other hand, frequency-division demultiplexing schemes have the advantage that only one cross-correlation must be performed for each spectral channel. Analogue filters have been used to split the wideband into sub-bands, but it has been difficult to 'stitch' the results together to yield the wideband spectrum because of the variability of the filters. In this Letter, a digital method based on the wideband interferometric digital architecture (WIDAR), is described and simulation results presented that permit the seamless stitching of bands. The wideband is sampled, split into sub-bands with digital filters, cross-correlated, and then stitched together. A block diagram for the WIDAR is shown in Fig. 1. A scheme is also described that acts in combination to effect fully digital sub-sample delay interpolation, which is required in order to achieve precision delay compensation [1].

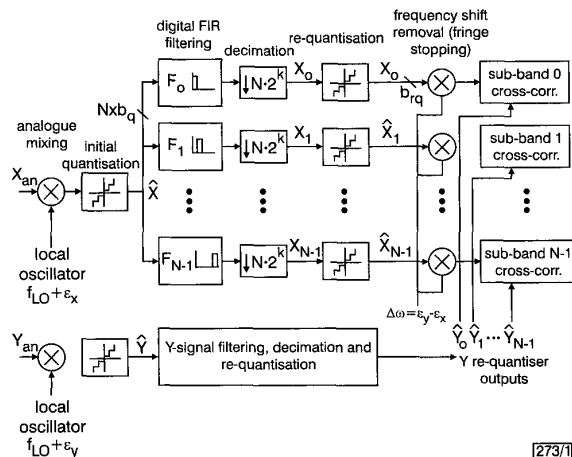


Fig. 1 Wideband interferometric digital architecture (WIDAR)

Filtering and decimation: A digital FIR filter has a predictable amplitude and phase response. The amplitude response is the Fourier transform of its tap coefficients provided that the internal word-length of the realised filter is sufficiently long. For a cosine-symmetric FIR, the phase is linear. If the integer sample delay through the filter is removed, then the phase is essentially zero down to the -15dB point in the transition band of a bandpass filter. These are the important qualities of filters for this application.

If the sampler output is time-demultiplexed by a factor of N , then decimation of the output of a particular FIR filter by the same factor (or $2^k \cdot N$; $k = 0, 1, \dots$) yields an efficient parallel architecture that must only operate at the decimated sample rate. Normally $k = 0$ but could be nonzero if it is desired to split the band into smaller sub-bands than the demultiplexing factor. For simplicity, $k = 0$ for the rest of the discussion. If the FIR filter has tap coefficients producing a bandpass of $1/N$ of the full band aligned to sub-band boundaries of n/N ($n = 0, 1, \dots, N-1$), then decimation by a factor of N will yield a baseband signal with bandwidth and sample rate reduced by a factor of N [2]. If n is odd, then the signal will have the opposite frequency sense and can be corrected by changing the sign of alternate samples. Any finite-length FIR filter will have a finite transition band. After decimation, the transition band outside the sub-band boundaries will alias with opposite frequency sense. False correlation of the aliased component will occur unless caused to decorrelate.

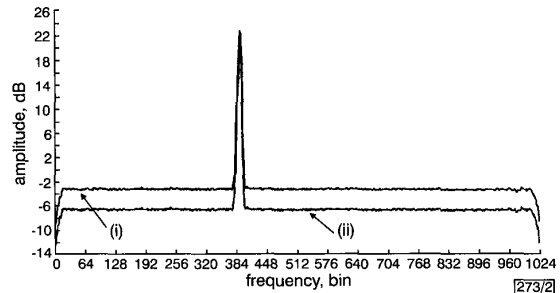


Fig. 2 Amplitude of reference full band and WIDAR correlation results

- (i) WIDAR correlation: Normalised broadband noise RMS: 0.00832
- (ii) Reference fullband correlation: normalised broadband noise RMS: 0.00827

General configuration: Original sample rate: 4Gsample/s; 500×10^6 samples simulated; identical noise generator seeds; Hanning windowing
 WIDAR configuration: 16 sub-bands; FIR filters: 1023 tap, cosine symmetric; 10 bit internal wordsize with block floating point; original quantisation: 4 bit; re-quantisation: 4 bit

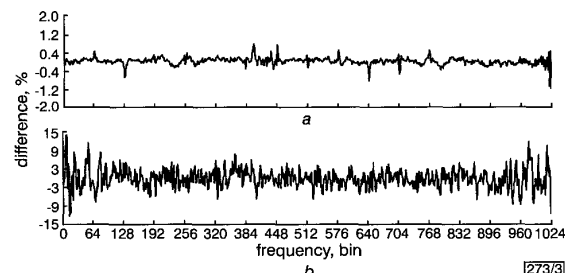


Fig. 3 Percentage difference between full band and WIDAR correlation

- a Identical noise generator seeds
- b Different noise generator seeds

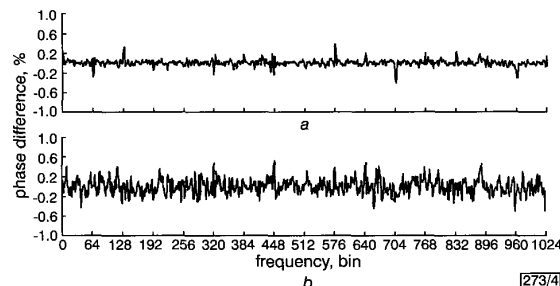


Fig. 4 Phase difference between full band and WIDAR correlation

- a Identical noise generator seeds
- b Different noise generator seeds

Correlation and power correction: With the WIDAR, false correlation can be prevented if the local oscillator in each interferometer element has a unique (perhaps artificially imposed) frequency shift ϵ that is removed after decimation. Since the frequency sense of